Inertial Sensing for Lateral Walking Gait Detection and Application in Lateral Resistance Exoskeleton

Lijun Yang, Kui Xiang, Muye Pang, Meng Yin, Xinyu Wu, *Senior Member, IEEE*, and Wujing Cao

***Abstract*— Lateral walking gait detection is necessary for the development of wearable devices applied to side stepping. To our knowledge, rarely work has been conducted to identify lateral walking gait by wearable sensors. Based on a hip exoskeleton, we presented a method for lateral walking gait phase detection only by two IMUs mounted on the shank. Experiments were conducted to detect narrow double support, swing of the leading leg, wide double support, and swing of trailing leg phases of 12 healthy subjects walking at various speeds. The performance of four different algorithms including thresholding (THR), modified *k*-nearest neighbor named urban buildings indexing (UBI), random forest (RF), and neural networks (NNs) was evaluated. The occupation of space resources of NN is the smallest besides THR. The total recognition accuracy [mean and standard error of the mean (SEM)] of the RF-based, UBI-based, and NN-based systems was 97.07% ± 0.07% (off-line), 96.64% ± 0.16% (off-line), and 95.22% ± 0.60% (real-time), respectively. The recognition time of the models based on RF, UBI, NN, and THR was 13.3 ± 1.1, 5.7 ± 0.5, 2.6 ± 0.2, and 0.8 ± 0.2 ms, respectively. The recognition accuracy (cross-subjects) of RF-based, UBI-based, and NN-based systems was 91.72% ± 0.42%, 89.63% ± 0.48%, and 89.60% ± 0.43%, respectively. The results demonstrated that the proposed method can be applied to lateral walking gait detection.**

***Index Terms*— Classification, gait phase recognition, hip exoskeleton, IMUs, lateral resistance walking.**

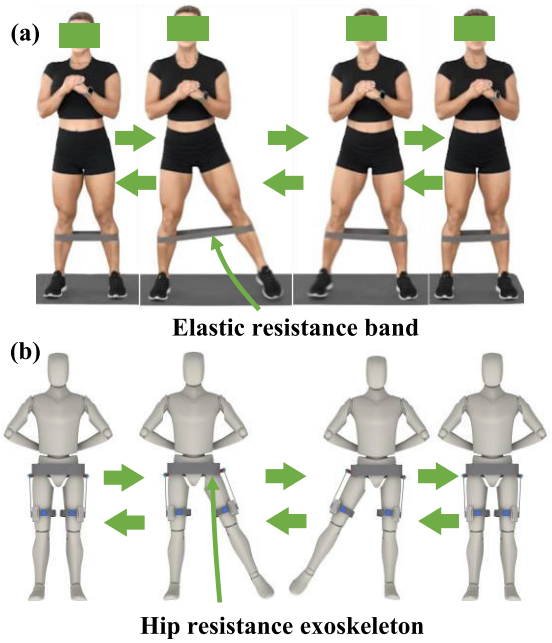

Fig. 1. Lateral walking with hip resistance exoskeleton to replace elastic band. (a) Lateral walking with elastic resistance band. (b) Lateral walking with hip resistance exoskeleton.

I. Introduction

LATERAL resistance walking is a popular hip abductor strengthening exercise. The conventional realization method is side stepping with an elastic resistance band secured around the lower extremities [1]. Lateral band walking is simple and easy to operate. Its disadvantages, however, are obvious: 1) in the initial phase, the elastic band has no force. The greater the swing of the leg the greater the resistance. This will make the muscles increasingly fatigued, which is the exact opposite of the actual form of muscle exercise. And this has a greater impact on the blood pressure; 2) during training, it is impossible to actively control the amount of resistance; 3) when training the muscles on one side of the leg (such as hip abductors), the muscles on the other side (such as hip adductors) are not subject to force; 4) it is necessary the person adapts to the force of the elastic band, rather than the reaction force of the equipment adapting to the person; and 5) it is not possible to provide individualized exercise for individual differences. In order to overcome these disadvantages and to facilitate the intellectualization and individuation of lateral resistance walking, our method is to apply resistance to the hip by exoskeleton during lateral walking, as shown in Fig. 1.

Lateral walking gait detection is a key premise for the application of hip exoskeleton in lateral resistance walking. In forward walking, the critical gait events heel strike and toe off are often used to identify stance and swing phases.

Manuscript received 2 November 2022; revised 14 February 2023; accepted 19 March 2023. Date of publication 6 April 2023; date of current version 19 April 2023. This work was supported in part by the Shenzhen Science and Technology Program under Grant JCYJ20220531100808018 and Grant RCBS20210706092252054, in part by the National Natural Science Foundation of China under Grant 62003327, in part by the Guangdong Basic and Applied Basic Research Foundation under Grant 2021A1515011699, and in part by the Shenzhen Institute of Artificial Intelligence and Robotics for Society. The Associate Editor coordinating the review process was Dr. Lihui Peng. *(Corresponding author: Wujing Cao.)*

Lijun Yang is with the School of Automation, Wuhan University of Technology, Wuhan 430062, China, and also with the Guangdong Provincial Key Laboratory of Robotics and Intelligent System, Shenzhen Institute of Advanced Technology, Chinese Academy of Sciences, Shenzhen 518005, China (e-mail: yanglijun@whut.edu.cn).

Kui Xiang and Muye Pang are with the School of Automation, Wuhan University of Technology, Wuhan 430062, China (e-mail: xkarcher@126.com; pangmuye@whut.edu.cn).

Meng Yin, Xinyu Wu, and Wujing Cao are with the Guangdong Provincial Key Laboratory of Robotics and Intelligent System, Shenzhen Institute of Advanced Technology, Chinese Academy of Sciences, Shenzhen 518005, China, and also with SIAT Branch, Shenzhen Institute of Artificial Intelligence and Robotics for Society, Shenzhen 518000, China (e-mail: wj.cao@siat.ac.cn).

Digital Object Identifier 10.1109/TIM.2023.3265105

Most lower limb exoskeletons (LLEs) for forward walking use pressure sensors to determine stance or swing, and IMUs to recognize the direction and velocity of walking [2]. However, lateral walking gait phase division is different from forward walking. To our knowledge, no work has been conducted for lateral walking gait detection by wearable sensor system for now.

The detection of lateral walking gait with inertial sensor alone has advantages of low physical complexity, small size, and high portability. A few algorithms and methods have been presented in LLEs and prosthesis to process inertial signals for forward walking gait detection. Kim et al. [3] used two IMUs on the anterior part of the thigh and thresholding (THR) method to detect gait event for hip assistance exosuit. Chen et al. [4] proposed a probability distribution model-based approach for foot placement prediction in the early swing phase with a wearable IMU sensor. Zhang et al. [5] presented a continuous phase estimation method based on a dual adaptive frequency oscillator by IMUs for LLEs. Zhong et al. [6] used foot and ankle IMUs to detect gait phase for a cable-driven exoskeleton aimed to improve gait symmetry. Among the algorithms and methods for inertial signals processing, peak identification [7] and THR [8] methods are the simplest and most straightforward. Some researchers have also tried neural networks (NNs) [9], feature extraction [10], hidden Markov models [11], [12], Gaussian mixture models [13], and other machine learning methods [14]. Although above researches are all for forward walking and cannot be transferred to lateral walking directly. Their thinking and methods have laid foundation of lateral walking gait detection by IMUs alone.

There have been many references and targeted improvements for the phase division and recognition algorithms in normal gait. The difficulty of this work is that there is no relevant recognition algorithm research for lateral walking. We need to research the suitable algorithm by ourselves. More importantly, the publicly available standard lateral gait dataset was not available. We also need to collect the gait dataset of lateral walking by ourselves. The above work is heavy and the cycle is long, but it is necessary.

The aim of this work was to present a real-time lateral walking gait detection method based on a trained model utilizing two IMUs of lateral resistance exoskeleton. The major contributions of this work are as follows.

1) To our knowledge, this is the first work to identify lateral walking gait phases only by two IMUs. Four lateral walking gait phases which are important for the lateral resistance walking exoskeleton were identified.
2) The algorithm performance of THR, modified k-nearest neighbor (KNN) named urban buildings indexing (UBI), random forest (RF), and NNs were evaluated. The real-time recognition accuracy of the NN-based system was 95.22% $\pm$ 0.60%. The recognition time of the models based on RF, UBI, NN, and THR was 13.3 $\pm$ 1.1, 5.7 $\pm$ 0.5, 2.6 $\pm$ 0.2, and 0.8 $\pm$ 0.2 ms, respectively.
3) The cross-subjects test was conducted. The recognition accuracy of RF-based, UBI-based, and NN-based systems was 91.72% $\pm$ 0.42%, 89.63% $\pm$ 0.48%, and 89.60% $\pm$ 0.43%, respectively.
4) An experiment to assess the effect of the hip exoskeletons on wearers in muscle activity was conducted. The gluteus medius (GMed) muscle activities in without wearing the hip exoskeleton (No-exo) and with the hip exoskeleton actively providing resistance (Exo-on) conditions were 3.9% $\pm$ 0.2% maximum voluntary isometric contraction (MVIC) and 8.7% $\pm$ 0.1%MVIC [mean $\pm$ standard error of the mean (SEM)], respectively. The tensor fasciae latae (TFL) muscle activities in No-exo and Exo-on conditions were 2.3% $\pm$ 0.1%MVIC and 20.6% $\pm$ 0.2%MVIC (mean $\pm$ SEM), respectively.

II. Methods

A. Experimental Platform and Equipment

The hip exoskeleton platform in this experiment was provided by Shenzhen Institute of Advanced Technology, Chinese Academy of Sciences, as shown in Fig. 2(a) and (b). This symmetrical exoskeleton has a size-adjusted mechanism to fully accommodate wearers of different heights and weights. Two high-power and low-inertial gimbal motor (GBM8008, DJI, China) are symmetrically mounted on the waist frame of the exoskeleton and deliver active resistance to hip abduction through elastic couplings and two connecting rods. In addition, the connecting rod parallel to the thigh and the metal connecting rod wrapping the buttock are connected by a pin shaft. It provides a passive DOF for hip flexion and extension during forward walking.

Two IMUs (LPMS-B2, Alubi, China), small and lightweight attitude sensor with nine-axis and capabilities of wirelessly transmitting data, were mounted on the shank of subject. The LPMS-B2 contains three sensors: a gyroscope, an accelerometer, and a magnetometer. Gyroscope and accelerometer are used in this experiment. The installation position of IMU is shown in Fig. 2(b) and (c). The x-axis of the IMU points to the direction of the subject's lateral walking, the y-axis of the IMU is perpendicular to the palm of the foot, and the z-axis of the IMU points to the toe. The pressure insole module (RX-ES-48P, RouXi Technology, China) is used to detect plantar pressure during lateral walking as a label for dividing gait phase. The control module of the exoskeleton consists of a micro controller unit (MCU) and an application processor unit (APU). The MCU is based on 168 MHz Cortex-M4 processor and the APU is based on 1.5 GHz Cortex-A72 (ARMv8) processing system. The MCU is used to collect IMU signals and plantar pressure signals, which are sent to APU via SPI. And then the APU performs real-time recognition of gait information. Eventually, the APU sends the recognition results, IMU signals, and plantar pressure signals together to the computer after packing to facilitate further analysis.

B. Lateral Walking Gait Phase Division

There are very few studies on lateral walking gait, and the way to divide the gait is not uniform. For example,

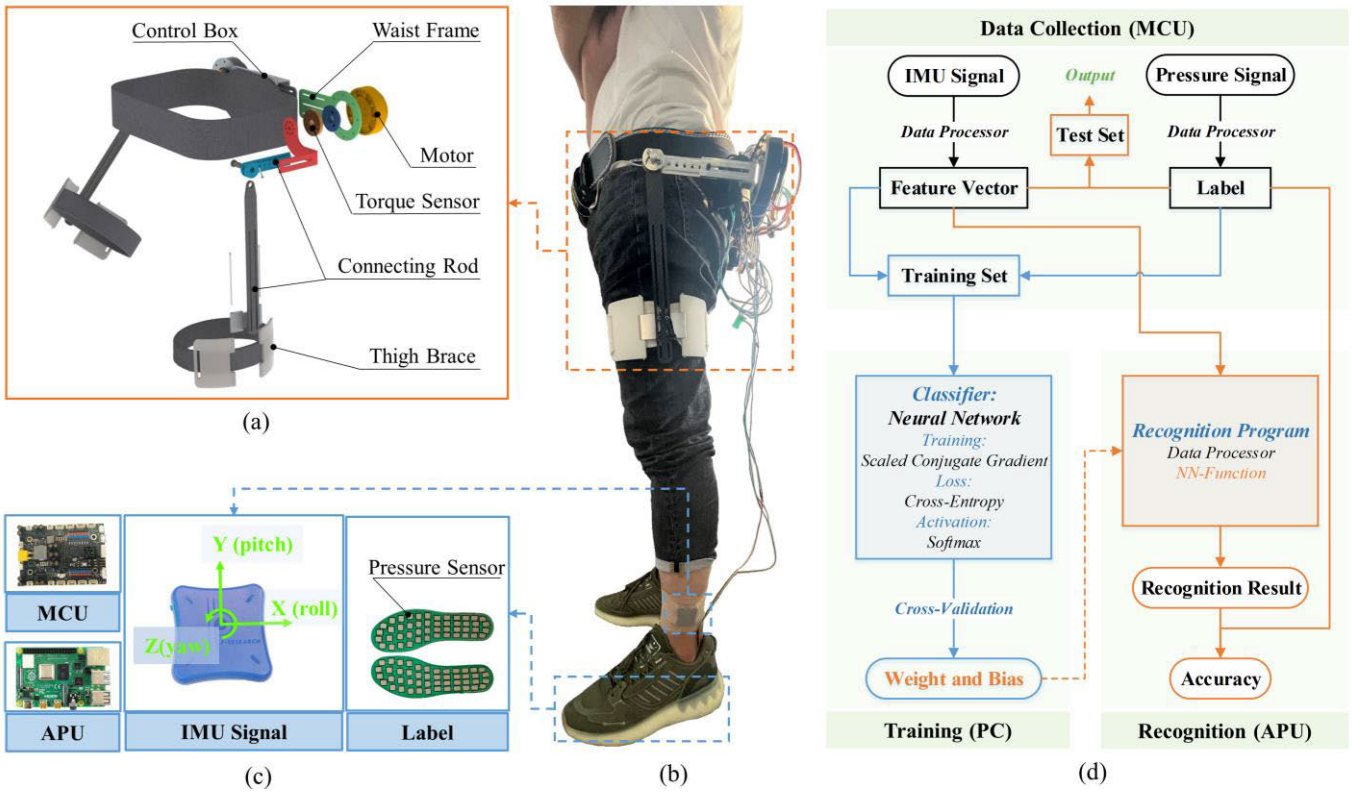

Fig. 2. Hip exoskeleton and identification system. (a) Major dimensions and components of the hip exoskeleton. (b) Prototype with wearer. (c) Sensors and control boards. (d) Flowchart for recognition system establishment.

Yamashita et al. [15] divided the lateral gait phase according to different lateral walking modes (walking, galloping, and running). Berry et al. [16] focused on lateral sidestepping and crossover stepping. Kuntze et al. [17] distinguished between lateral strides in an upright and squat posture. Compared to them, we are dividing the lateral gait according to the project task. And our division is sufficient for lateral resistance walking. In this study, the left leg is the leading leg and the right leg is the trailing leg. A complete gait cycle can be divided into different gait stages according to typical gait events during walking [18]. As shown in Fig. 3, a complete lateral walking gait cycle was defined for this study. Gait cycle starts with trailing foot contacts ground (TFCG). At this point, both legs stand almost straight and body weight gradually shifts from leading to trailing legs. This stage is defined as narrow double support (NDS, phase 1). As the weight gradually moves from leading leg to trailing leg, leading leg gradually lifts. The instant of leading foot off (LFO) the ground is regarded as the end of phase 1 and the opening of phase 2, which is defined as the swing of the leading leg (SLL, phase 2). Leading foot contacts ground (LFCG) marks the end of phase 2. Next, enter a stage called wide double support (WDS, phase 3). During this phase, the legs stand apart and the body center of gravity gradually shifts to the leading leg. When the body center of gravity is fully transferred to the leading leg, the trailing leg off (TFO) the ground and moves from phase 3 to phase 4. This phase, which continued into the TFCG, was defined as swing of trailing leg (STL, phase 4). As can be seen in Fig. 3(b), the lateral roll curve of the leading leg and the lateral roll curve of the following leg are reversely symmetrical with respect to the middle of the NDS or WDS phase. That is, starting from the middle of the NDS or WDS phase (the intersection point of the two curves), one of the two curves goes forward and one goes backward. It can be seen that they show a symmetrical trend. This trend was consistent with the predicted change in the Angle of both legs during lateral walking.

In this study, the plantar pressure signal is used as a label for the occurrence of gait events, and then the gait cycle is divided into different gait stages based on these labels. Gait phase divided based on plantar pressure are regarded as actual classes. Correspondingly, gait phase divided by recognition systems based on signals of IMUs is regarded as predicted classes.

This following experiment can be divided into three stages: 1) collection of experimental data; 2) establishment of recognition system; and 3) performance evaluation of the system. The subjects were asked to walk laterally in different speeds during the experimental data collection periods. Then the posture data of their legs were collected to prepare for the follow-up work. In the establishment stage of the identification system, these pose data need to be screened and processed to extract feature vectors. This feature training is then used to train immature models. Finally, these trained models are transplanted into the recognition system to identify the gait phase of lateral walking.

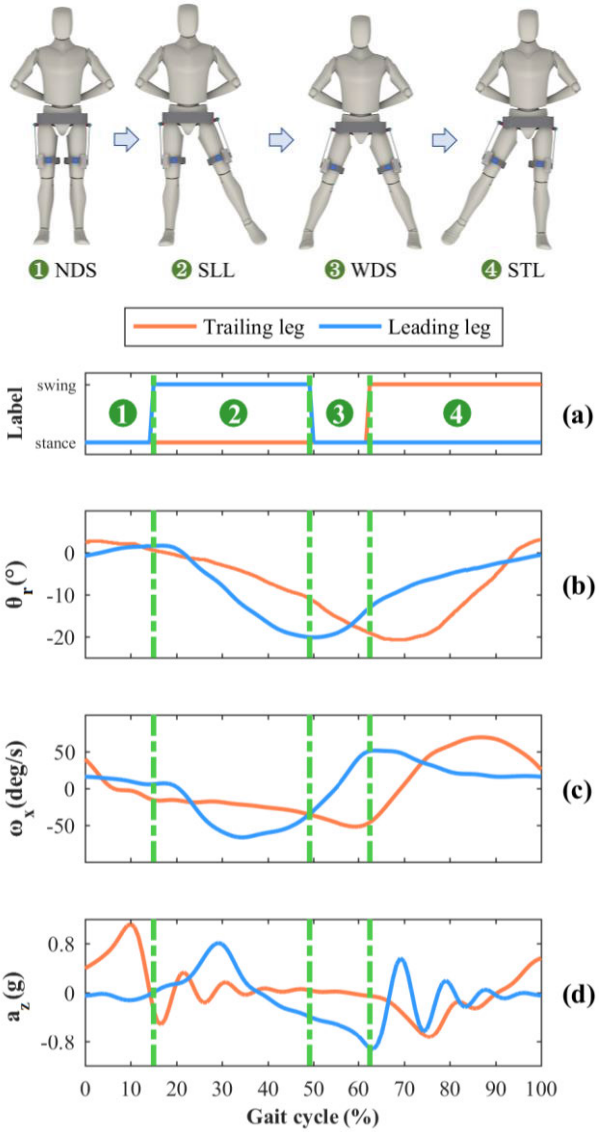

Fig. 3. Lateral walking gait division. (a) Labels derived from plantar pressure. (b) Variation curve of angle of roll under single gait cycle. (c) Variation curve of angular velocity of x-axis under single gait cycle. (d) Variation curve of linear acceleration of z-axis during a single gait cycle.

C. Collection and Processing of Data

In this study, the IMUs signals of nine channels are collected as raw data: three tilt angles (roll, pitch, and yaw), angular velocity, and linear acceleration in the x-axis, y-axis, and z-axis, respectively. At the same time, plantar pressure signals are collected as labels. The MCU is used to synchronously collect the posture signal and plantar pressure signal of the experimental subject during the experiment in real-time. Among these signals, the attitude signal is sent by the IMU through Bluetooth technology, and the foot pressure signal is sent by the pressure sensor through a universal asynchronous transceiver (UART). The signal acquisition frequency is 100 Hz.

Twelve adults were recruited to complete the designed experimental tasks. They were required to sign an informed consent prior to participate in the experiments. This study was approved by the Medical Ethics Committee of Shenzhen Institute of Advanced Technology (SIAT-IRB-200715-H0512, valid time from January 2020 to December 2022). They were divided into two groups, A and B. Group A consists of nine subjects whose experimental data are all included in the training set to generate the recognition model and classifier. Group B included three subjects who underwent two experiments. The data from the first experiment were included in the training set, and the second experiment was a real-time recognition test of their lateral gait. Before the experiment, we conducted the necessary training for each subject to acclimate to experimental process. Before starting each data acquisition, participants were asked to stand in the initial position in the NDS phase pose in order to zero the IMU device with the upper computer. This addressed the error due to the experimenter's installation of the IMU. In this experiment, subjects were asked to walk laterally in three different modes. The three modes are fast (0.4 m/s), slow (0.26 m/s), and "normal speed" (the normal speed as perceived by the participants), which needs to be conducted twice (30 steps of lateral walking are required each time). After each trial, the subjects need to return to the origin to prepare for the next experiment. The whole experiment was conducted on the flat ground. We used a metronome to control the subject's stride frequency and marked the ground to control the subject's stride length (50 cm).

Above collected data need to be filtered and processed before it can be used to train the model. Dispersion, redundancy, and correlation are all important metrics for screening data. In this study, the function xcorr in MATLAB was used to correlate the signal to eliminate some redundant signal paths. The signals of three channels were retained: roll, angular velocity of x-axis, and linear acceleration of z-axis. Among them, the roll angle was zeroed according to the collected data of the subject at the initial position to reduce the influence of IMU position error on the signal.

In addition, the Kalman filter is used to filter the signals of these channels for removing noise from the signals. Processed data are shown in Fig. 4. In this experiment, we use a sliding window to extract the characteristics of the signal. Since the duration of each phase of the lateral gait is less than 0.8 s, the length of the sliding window is set to 800 ms, and the sliding increment is 10 ms. The time domain features of the filtered data are extracted, mainly including: maximum value (Max), minimum value (Min), zero crossing (ZC), variance (VAR), and mean. They are composed in vector form into the training set (181 350 $\times$ 30). They included data for three modes of fast, slow, and "constant speed" for subjects in groups A and B. These data were used to train the model and make the model more capable of gait recognition for lateral walking. Finally, the mature model is converted into a classifier dedicated to classification work, which is used to implant the corresponding recognition system for real-time recognition experiments. Fig. 2(d) shows the generation process of the recognition system. We take NN as an example to introduce how it is integrated into the recognition system. First, based on the MCU, the subject's posture data and plantar pressure data are collected by the IMU and pressure sensors. These

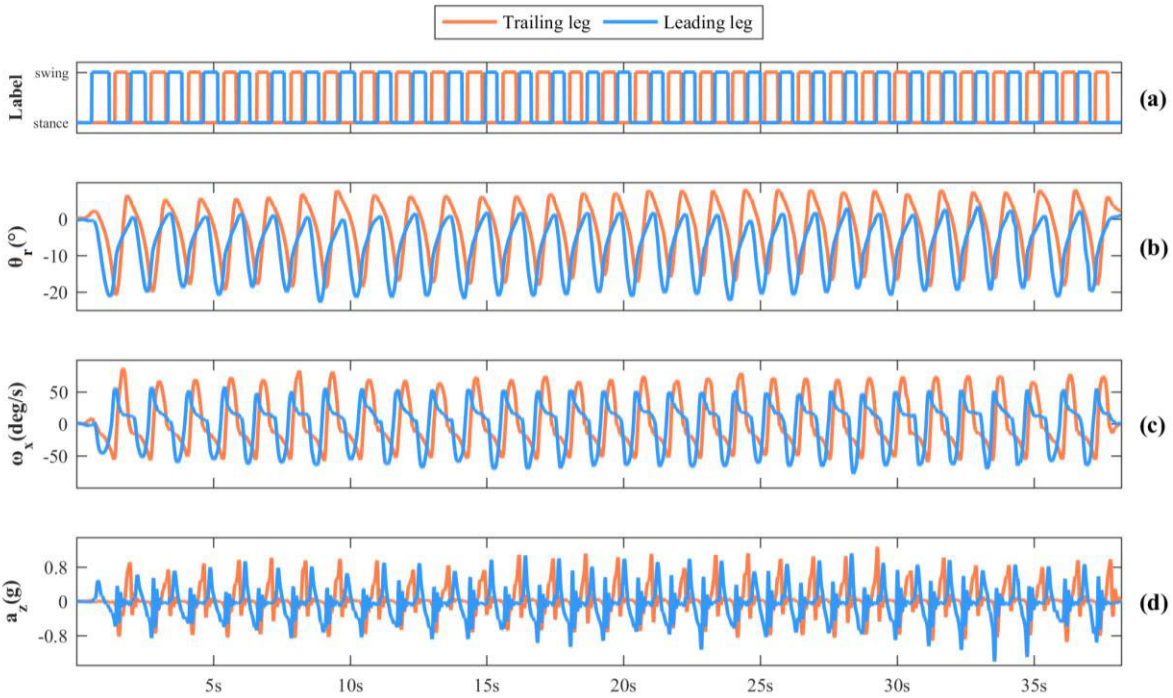

Fig. 4. Filtered IMU signal. (a) Labels derived from plantar pressure. (b) Variation curve of angle of roll. (c) Variation curve of angular velocity of x-axis. (d) Variation curve of linear acceleration of z-axis.

data are then processed by the corresponding programs to form a training set. The training set is then imported into MATLAB. The training set contains feature vectors and labels, which are randomly partitioned into three groups: training (70%), validation (15%), and testing (15%). The number of hidden layer neurons is set to 30. The training method uses scaled conjugate gradient (SCG). Cross-Entropy is used as the loss function. Sotfmax was used as the activation function, and tenfold cross-validation was used. After the training is completed, the mature model is derived and the specific parameters in the model are extracted. These parameters include the weight matrix (30×30) and offset matrix (30×1) for the hidden layer, the weight matrix (1×30) and offset matrix (1×1) for the output layer, offset, gain, etc. Immediately after, the NN-based classification function NN-Function is written by applying these specific parameters. After that, this function is composed of the recognition program together with the signal processing function. Finally, the data of group B members are collected and their feature vectors (1×30) are input into the NN-Function function to get the recognition results. Then the labels are combined to get the accuracy rate. At the same time, the data of group B members are packaged into a test set and provided to other algorithms for testing.

D. Recognition Algorithm

The choice of the recognition algorithm is crucial. Some recognition algorithms have been designed by researchers to deal with different scenarios. These algorithms have achieved considerable results and high accuracy in their fields of expertise. Since there is no reference in the field of lateral walking gait recognition by IMUs, it is difficult to determine which algorithm is more friendly to lateral walking gait recognition before the experiment. For these reasons, various mainstream recognition algorithms will be used for reference and comparison. First, the filtered data and pressure signals are imported into MATLAB to generate corresponding feature vector sets and labels. Second, the recognition algorithms in the MATLAB platform are used to train and test the feature vector set based on the labels. Finally, the results of preexperiment, which only have relative reference significance, are shown in Table I. The accuracy of some types of algorithms is awfully unsatisfactory. By contrary, KNN, decision tree, and NNs showed anticipated potential. Therefore, they were selected for corresponding transformation and finally used to design the recognition system. In order to further understand the performance of these algorithms, a specific THR was developed to compare with the above three algorithms. Ultimately, four suitable algorithms were selected for designing the recognition system: THR, UBI (evolved from KNN, explained subsequently), RF (a kind of decision tree), and NN.

1) Thresholding: The establishment process of THR is as follows: Based on the collected data and labels, time domain features of signals closely related to specific events are identified. These selected features are used to design appropriate THR according to the certain logic which will be written into a program for discriminating the target. The results of the gait phase division according to the labels are shown in Fig. 3. It can be clearly observed that the corresponding signals of IMUs have distinct characteristics at the demarcation line between different gait phases. As shown in Fig. 5, a schematic of the THR algorithm for gait division is presented. The used THR is based on feature factors which include four kinds of

TABLE I
SELECTION OF ALGORITHM (ACCURACY: %)

Linear Discriminant	Quadratic Discriminant	Subspace Discriminant
78.7	87.9	84.3
Linear SVM	Quadratic SVM	Subspace KNN
91.4	92.3	95.2
Coarse KNN	Medium KNN	Fine KNN
93.8	95.3	96.5
Cosine KNN	Cubic KNN	Weighted KNN
94.5	95.1	96.5
Simple Tree	Medium Tree	Complex Tree
80.0	88.9	90.9
Boosted Trees	Bagged Trees	Rusboosted Trees
91.0	96.7	86.8
Neural Network	NARX Network	NIO Network
95.4	90.5	93.3

Notes: Support Vector Machines (SVM), Nonlinear Autoregressive with External Input (NARX), Nonlinear Input-Output (NIO)

data: time, the max/min value of the roll angle of the two legs and the max/min value of the difference between them, the max/min value and the ZC of the angular velocity of the x-axis, and the max/min value and the ZC of the linear acceleration of the z-axis. We take the detection of SLL as an example. First, when the feature factors related to the lateral roll angle of both legs appear, it is detected by the feature factors monitor. Then the detector is passed to the feature factors accumulator, which causes the accumulator to add 1. Similarly, the feature factors related to the angular velocity of the X-axis and the linear acceleration of the Z-axis are detected when they appear. When the value of the accumulator exceeds a given value (4 in this article), the feature factors accumulator outputs the corresponding gait events, such as front-foot swing and rear-foot stance. At the same time, the program needs to check if the time factor satisfies the condition. Finally, after satisfying above conditions, the gait phase divider derives the gait phase as SLL according to the combined mode of gait events of both legs. Similarly, using this approach, other stages of gait phase can be identified.

2) Urban Buildings Indexing: Since the KNN requires numberless sorting work, as the amount of data becomes larger and larger, this work will become more and more difficult for MCU. So that, in the later stage, the model designed with KNN will not achieve the effect of fast real-time recognition. However, inspired by the idea of the KNN, the author of this article has developed a search model named "UBI" which can perform fast real-time identification. The so-called "UBI" refers to, in the MCU, a special and preestablished database which is composed of a 2-D array and a group of 1-D arrays. The address pointer is stored in the 2-D array which is similar to the land of a city. The array subscript is used to number each address, so that the address pointer in the array can be

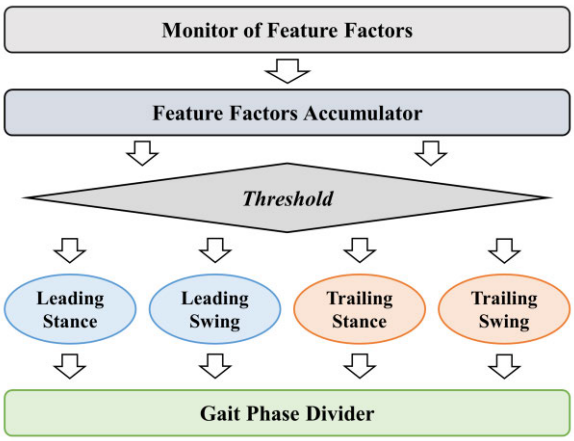

Fig. 5. Schematic of THR algorithm for gait phase division in lateral walking.

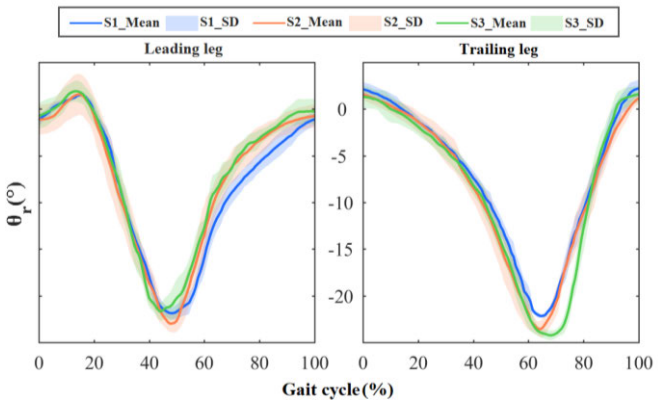

Fig. 6. Roll curve (mean and SD) of single gait cycle of three subjects in group B.

quickly retrieved. Significantly, these address pointers point to different 1-D arrays which are similar to high-rise buildings located in a city. The 1-D arrays store preclassified values arranged in order. From a certain point of view, the entire database can be considered as a 3-D database. When a 3-D data is given, such as the IMU signal, the model can quickly query the category of the value closest to the signal by using the array subscripts in the 3-D database to determine the class of the signal.

Compared to the traditional KNN approach, UBI differs in that the traditional 2-D addressing is changed to 3-D addressing. It makes UBI take up less space than the traditional KNN, but the speed decreases. The construction of the UBI model requires abundant training data. In this article, it refers to the signals of the three channels of the IMU after filtering. The model construction process is as follows.

1) First, two of the three channels of data are used to build the city's land (2-D array). According to the variation range of the two data, it is divided into M parts and N parts with certain rules and proportions. Meanwhile, M and N, respectively, correspond to the two dimensions of the 2-D array.
2) Second, the remaining data in the three channels are also divided into several parts according to certain

rules. A sequential linked list is established on the corresponding 2-D array address. This can speed up model building.

3) Finally, in order to save storage space, the values in the sequential linked list need to be extracted and reconstructed into a 1-D sequential array.

3) Random Forest: RF was formally proposed by Breiman [19] in machine learning. RF is a decision tree algorithm. Its basic idea is that multiple decision trees perform the decision task together to compensate for the lack of capability of a single decision tree. The RF algorithm used in this article was proposed by Raileanu and Stoffel [20] in Annals of Mathematics and Artificial Intelligence. It is based on the Gini coefficient (a concept in the field of economics, an indicator used to judge the fairness of income distribution, with a value between 0 and 1) as a criterion to select attributes for division. The equation of this Gini coefficient is

$$\text{Gini}(D) = 1 - \sum_{k=1}^{N} p_k^2 \tag{1}$$

where $D = \{(x_1, y_1, z_1), (x_2, y_2, z_2), \ldots, (x_n, y_n, z_n)\}$ is the sample set, N is the total number of sample classes (in this experiment, $N = 4$) and p_k is the proportion of samples in category k ($0 \le p_k \le 1$, $\sum_{k=1}^{N} p_k$). The smaller the Gini (D), the higher the purity of the sample set.

4) Neural Networks: A typical NN algorithm mainly includes input layer, hidden layer, output layer, neuron, and weights. The main principle of the NN is to continuously adjust the value of the weight through appropriate strategies, so that the output value obtained by combining them with the input according to the given rules will constantly approach the expected output value. The inputs of the neurons are transformed into outputs by an activation function. The NN eventually selected is the Back Propagation Neuron Network, and its training method is the SCG. It contains two hidden layers, and the activation function adopts the Softmax. Its equation is as follows:

$$\text{Softmax}(h_i) = \frac{\exp(h_i)}{\sum_j \exp(h_j)} \tag{2}$$

where h is input of neurons, h_i and h_j are one of the elements in the input. In order to simplify the problem, the output is converted from the original 4×1 vector to the 2×2 vector, so the four-classification problem is split into two two-classification problems. In this study, the loss function adopts the cross-entropy. For the cross-entropy of binary classification problem, the loss function can be simplified into the following form:

$$L(y', y) = -[y \ln y' + (1 - y) \ln(1 - y')] \tag{3}$$

where $y'(y' = \text{softmax}(h))$ is the probability of the model predicts that the sample is a positive example and y is the sample label (if the sample belongs to a positive example, its value is 1, otherwise the value is 0).

E. Principle of System Performance Evaluation

The performance of the recognition system is evaluated using the repeatability of signals, time performance, space resource occupancy, and recognition accuracy.

1) Repeatability of Signals: Similar to normal gait, lateral walking gait is a periodic movement. Therefore, in this article, the variance ratio (VR), which is commonly used to describe the repeatability of normal gait signals [21], [22]. It was also used to assess the lateral walking gait. In order to standardize the data and make the amount of data in each gait cycle consistent, each set of experimental data of the three members of group B was cut into 30 steps according to the label (30 steps for each group). The data for each step is then interpolated. The formula for calculating VR is as follows [23]:

$$\text{VR} = \frac{\frac{1}{n}\sum_{i=1}^{n}\left(\frac{1}{N-1}\sum_{j=1}^{N}(X_{ij} - \overline{X}_i)^2\right)}{\frac{1}{n-1}\sum_{i=1}^{n}\sum_{j=1}^{N}(X_{ij} - \overline{X})^2} \tag{4}$$

where n represents the amount of data in a single gait cycle, N represents the number of steps, X_{ij} represents the value of the roll angle of the ith leg in the jth step, $\overline{X}_i$ is the average value of the ith data point in step N, and $\overline{X}$ is the average value of the gait cycle $\overline{X}_i$.

2) Time Performance: Model training time and recognition time are included in the time performance. Training time is the amount of time spent importing the training data set into the initial model, training, and producing the mature model. The recognition time is divided into real-time recognition time and off-line recognition time. The IMU signals collected online are filtered and integrated into feature vectors, then imported into the classifier, and finally the classification results of the signals are obtained. The time required for this whole process is called real-time recognition time. The only difference between the off-line recognition time and the real-time recognition time is that the recognition procedure takes place off-line.

3) Occupation of Space Resources: The space resources occupied by the identification system mainly include three parts, they are: the space resources occupied by the code of the whole system before the program runs, the space resources occupied by the input data in the process of the program running, and the extra space resources temporarily occupied by the program running. Due to the different algorithms used in the models, the space resources occupied by the recognition systems are also different. It is necessary to calculate the space occupied by the system in order to understand the performance of these recognition systems.

4) Recognition Accuracy: Recognition accuracy includes the total accuracy of the model for the whole gait recognition and the prediction accuracy of the model for each class (each gait phase). In this article, the confusion matrix is considered to calculate the accuracy. The certain value of confusion matrix is calculated according to (5), and the calculation method of

total accuracy is defined in (6)

$$\text{Prediction}(i, j) = \frac{N_{ij}}{N_i} \tag{5}$$

$$\text{Accuracy} = \frac{\sum_{i=j}^{K} N_{ij}}{N} \tag{6}$$

where K is the number of categories and $K = 4$ for the four-class problem. The i represents the ith class in the actual class (class represented by the label) and the j represents the jth class in the predicted class (i and j take values of 1, 2, 3, and 4). N_{ij} is the number of class i predicted as class j, and N_i is the total number of actual class i. Prediction (i, j) is the probability that class i is predicted as class j in each class i. When $i = j$, Prediction (i, j) refers to the prediction accuracy of class i. Accuracy is the proportion of the correct number $(i = j)$ of predictions over the total number, that is, the total accuracy.

III. Results

In this experiment, group A had a total of 32 valid datasets, all of which were used to form the training dataset. Among them, there are 11 data sets in fast mode, 13 data sets in slow mode, and 8 data sets in "normal speed" mode. Subjects in group B had nine sets of valid data in the first experiment (invalid data were not used for discussion due to errors in experimental operation and experimental equipment), and three sets of data for each of the three speed modes. They are used to join training datasets. After the system was established, we conducted a second experiment with three members of group B. First, the model established based on the NN algorithm is used to identify and classify the IMU signals in the "normal speed" mode of group B members online. After real-time recognition, this data are used to perform offline identification, based on models developed by other algorithms (RF, UBI, and THR).

A. Repeatability of Signals

In this experiment, VR was used to evaluate the repeatability of the roll signal; the value of VR is between 0 and 1, with higher values indicating more dispersed and less reproducible data. According to formula (4), the VR of S1, S2, and S3 were 0.025, 0.048, and 0.029 (leading leg) and 0.021, 0.30, and 0.18 (trailing leg), respectively. We plotted Fig. 6 to show the repeatability of the roll angle signal more intuitively. In this figure, S1, S2, and S3 represent the three subjects in group B and are shown in blue, orange, and green, respectively. The mean of the roll angle is represented by the solid line, and the standard deviation (SD) of the roll angle is represented by the shaded area. As can be seen from Fig. 6, the changing trend of the three participants' roll angle is almost the same, and the signal repeatability of S2 is the worst among the three.

B. Training and Recognition Time

The off-line training time is mainly related to the size of the training data set and the algorithms used in the designed model. In order to reduce the influence of the experimental equipment and other factors on the training time, the same equipment is selected to measure training time. The training data set consists of feature vectors. As described above (data filtering), data from six channels of two IMUs (three channels are selected for each IMU) are composed of a feature vector. In the off-line training phase, about 200 000 feature vectors of 12 subjects were used to train the model. In this study, there are four algorithms selected to build the model, three of which have a training time can be measured. As shown in Fig. 7, the blue part represents the training time, and the RF, UBI, and NN are 142, 38, and 54 s, respectively.

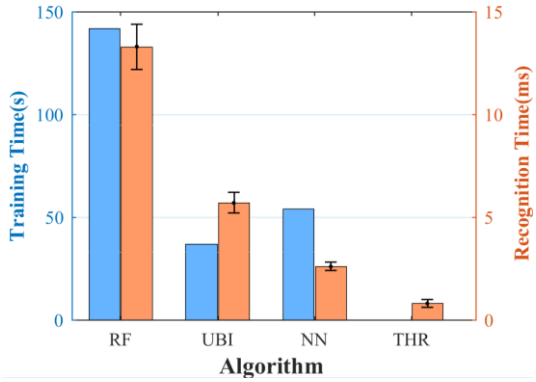

Fig. 7. Time performances based on RF, UBI, NN, and THR. The blue part represents the training time and the orange part represents the recognition time.

TABLE II
Occupation of Space Resources

Space	Algorithm			
	RF	*UBI*	*NN*	*THR*
P1	1144KB	628KB	17KB	10KB
P2	80B	80B	80B	120B
P2	816B	736B	1656B	588B

The working process of recognition system includes signal collection, data filtering, feature vector preparation, and recognition. The frequency of signal collection is 100 Hz, which is 10 ms, and the time of data filtering and feature vector preparation is less than 1 ms. For different recognition models, the time of these steps is the same, so here we only compare the time of the recognition process of different models. These results of recognition time are summarized in the orange part of Fig. 7. The mean recognition time of the models based on RF (off-line), UBI (off-line), NN (real-time), and THR (off-line) algorithms are 13.3 ± 1.1, 5.7 ± 0.5, 2.6 ± 0.2, and 0.8 ± 0.2 ms, respectively.

C. Occupation of Space Resources

In order to more clearly describe the spatial complexity of the system in tables, some abbreviations are necessary to declare in advance. The space occupied by the code before the entire system runs is denoted as P1. The space occupied by input data while the system is running is denoted as P2. The additional space temporarily occupied while the system

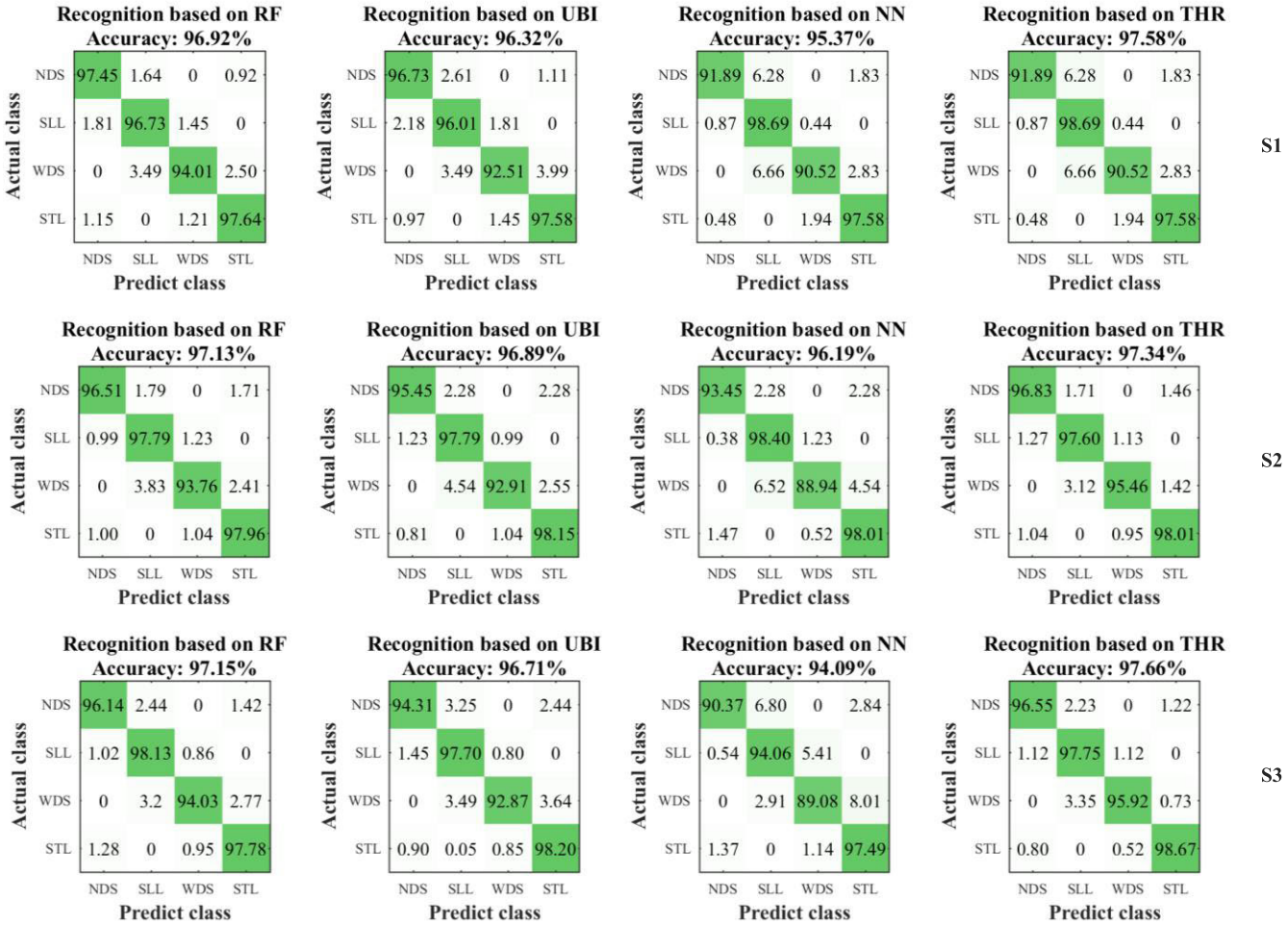

Fig. 8. Confusion matrix of gait recognition accuracy based on RF, UBI, NN, and THR.

is running is denoted as P3. As shown in Table II, the size of space resources occupied by the RF-based system is: P1 = 1141 kB, P2 = 80 B, and P3 = 816 B; the size of space resources occupied by the UBI-based system is: P1 = 628 kB, P2 = 80 B, and P3 = 736 B; the space resources occupied by the NN-based system is: P1 = 17 kB, P2 = 80 B, and P3 = 1656 B; and the space resources occupied by the THR-based system is: P1 = 10 kB, P2 = 120 B, and P3 = 588 B.

D. Recognition Accuracy

The recognition accuracy of the four recognition systems is measured based on the same data, in order to objectively compare their performance, and the accuracy of the system based on NN algorithm is measured real-time, the accuracy of the other three systems is measured off-line. In this experiment, the subjects' lateral gait signals are divided into four classes by the recognition system, which are NDS, SLL, WDS, and STL. The confusion matrix for class results is shown in Fig. 8, which contains the test results of three subjects (S1, S2, and S3) under four different recognition systems. Obviously, the accuracy of the whole gait recognition is above 95% except for the recognition accuracy (94.09%) of S3 based on NN algorithm system.

TABLE III
CONFUSION MATRIX BASED ON NN (%)

	NDS	SLL	WDS	STL
NDS	91.90±0.87	6.09±0.47	0.00	2.02±0.42
SLL	0.60±0.14	97.05±1.48	2.36±1.53	0.00
WDS	0.00	5.36±1.22	89.51±0.49	5.13±1.51
STL	1.11±0.31	0.00	1.20±0.40	97.69±0.16

The recognition results of the system based on NN algorithm are summarized in Table III. It can be seen that the system has the highest recognition accuracy to STL and the lowest recognition accuracy to WDS. In addition, NDS was mistaken for SLL (6.09% ± 0.47%), WDS was mistaken for SLL (5.36% ± 1.22%) and STL (5.13% ± 1.51%), and the rates of these errors were higher, exceeding 5%.

For the sake of comparing intuitively the recognition accuracy of these systems for different gait phases, we separately draw the recognition results of gait phases into a column chart. As shown in Fig. 9, the recognition accuracy (mean and SEM) of the four recognition systems (RF, UBI, NN, and THR) for gait phase NDS was 96.70% ± 0.38%, 95.5% ± 0.6%, 91.90% ± 0.87%, and 96.99% ± 0.30%, respectively. The recognition accuracy of gait phase SLL was 97.55% ± 0.42%,

TABLE IV
CONFUSION MATRIX OF S1, S2, AND S3

		NDS	SLL	WDS	STL
		Predict class			
RF	NDS	89.90±1.28	7.61±1.43	0.00	2.48±0.75
	SLL	2.61±0.17	92.83±0.24	4.53±0.45	0.04±0.01
	WDS	0.00	4.97±0.38	88.91±1.12	6.12±1.02
	STL	2.28±0.27	0.08±0.04	5.16±1.67	92.49±1.59
	Total	91.72±0.42			
UBI	NDS	88.66±3.03	10.35±2.93	0.00	0.99±0.76
	SLL	3.82±0.70	88.36±1.06	7.81±1.76	0.00
	WDS	0.00	4.50±2.61	93.71±2.00	1.78±0.76
	STL	3.9± 0.88	0.44±0.36	6.16±0.84	89.44±1.49
	Total	89.63±0.48			
NN	NDS	84.93±2.14	9.24±1.42	0.98±0.49	4.85±0.45
	SLL	4.68±0.83	90.28±0.40	4.69±0.99	0.34±0.23
	WDS	0.05±0.04	5.84±1.13	87.79±1.21	6.33±1.40
	STL	3.82±1.04	0.06±0.05	3.49±1.28	92.63±0.96
	Total	89.60±0.43			

Actual class

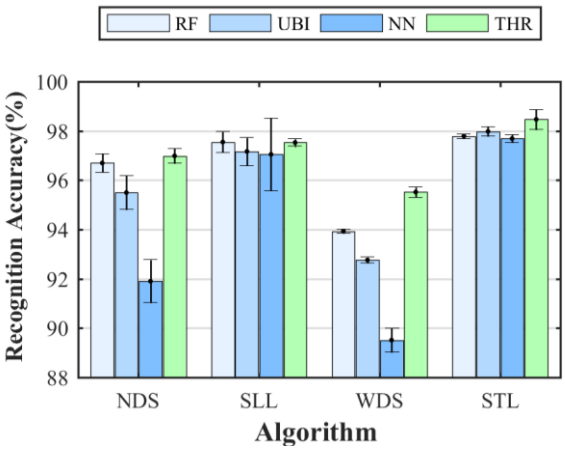

Fig. 9. Recognition accuracy (mean ± SEM, the subjects included S1, S2, and S3) based on four algorithms for different gait phases.

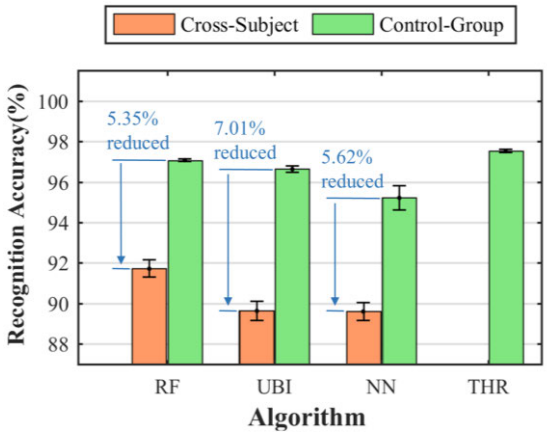

Fig. 10. Accuracy performance based on cross-subject. The orange part represents the recognition accuracy based on cross-subject and the green part represents the recognition accuracy of control-group.

97.17% ± 0.57%, 97.05% ± 1.48%, and 97.53% ± 0.15%, respectively. The recognition accuracy of gait phase WDS was 93.93% ± 0.08%, 92.76% ± 0.12%, 89.51% ± 0.49%, and 95.52% ± 0.21%, respectively. The recognition accuracy of gait phase STL was 97.79% ± 0.08%, 97.98% ± 0.19%, 97.69% ± 0.16%, and 98.47% ± 0.23%, respectively.

IV. DISCUSSION

A. Time, Space, and Accuracy

Due to the particularity of the THR algorithm, many parameters need to be set by the designer, and the training time of the system based on it cannot be measured. However, the recognition time is much lower than other systems, as shown in the orange section in Fig. 7. In addition, since the RF algorithm's strategy is to obtain results by voting on multiple decision trees, the time performance of its corresponding system is relatively unsatisfactory. As shown in Fig. 7, RF-based systems have much longer training times and recognition times than other systems. In contrast, both UBI-based and NN-based systems have better temporal performance, and the difference between the two is that, as shown in Fig. 7, the training time of the former is shorter than that of the latter, while the recognition time of the former is longer. It should be added that for real-time recognition, the recognition time of the system must be less than the sampling interval. In this experiment, the sampling interval is 10 ms, and the RF-based system recognition time exceeds this time, which means that the RF-based system cannot achieve real-time identification. Reassuringly, other systems can identify in real time.

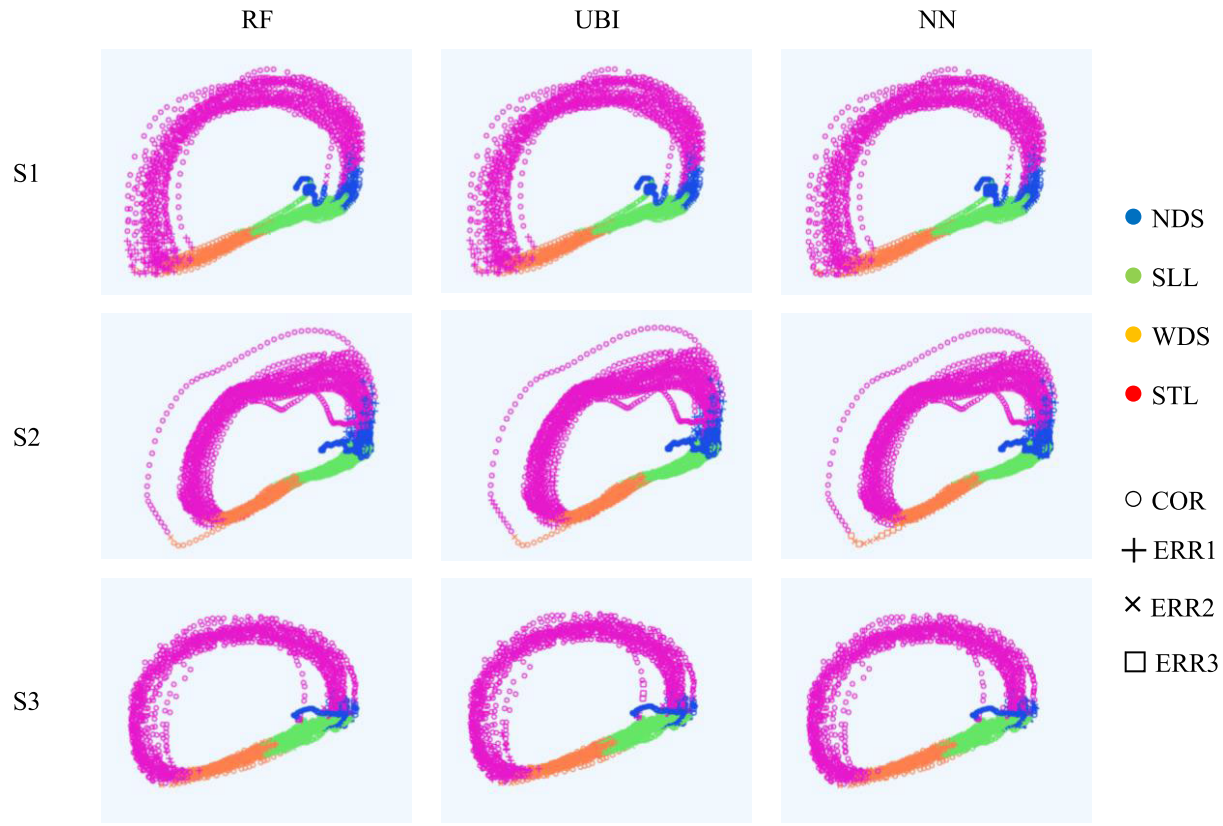

Fig. 11. Lateral walking gait visualization of S1, S2, and S3 based on RF, UBI, and NN. The different colors represent different gait phases. COR refers to predicting the correct gait phase, ERR1 and ERR2 refers to mistaken for adjacent gait phases and ERR3 refer to mistaken for alternating gait phase.

The space resources of the four recognition systems are different since the difference of the ideas among the four algorithms. It is only a few kilobytes of space occupied by NN-based and THR-based systems, while RF-based and UBI-based systems take up hundreds or even thousands of kilobytes, as shown in Table II.

On the contrary, the recognition accuracy of these systems (except for THR-based system) shows an opposite trend compared with their time performance and space complexity. The total recognition accuracy (mean and SEM) of the RF-based, UBI-based, and NN-based systems was 97.07% ± 0.07%, 96.64% ± 0.16%, and 95.22% ± 0.60%, respectively, as shown in the green part of Fig. 10. They are gradually reduced, which is contrary to their temporal performance and spatial complexity. A combination of other algorithms and sensor signals can be used for lateral walking gait detection. Ryu et al. [24] compared KNN, LDA, and QDA in gait phase detection, and the method of KNN was not inferior to the other two methods. Shi et al. used the methods of KNN, support vector machine (SVM), and RF to identify gait and demonstrated the superior performance of RF [25]. Huang et al. [26] and Hasan et al. [27] both improved CNN and used it to design gait recognition models with satisfactory accuracy. In addition, the recognition accuracy of THR-based system (mean and SEM) is 97.53% ± 0.09% in this work, as shown in the green part of Fig. 10, which is the highest of all recognition systems. This is consistent with the findings of Bejarano et al. [28] and Rueterbories et al. [29], all of which have high-level of accuracy. Although the study of this experiment is lateral gait, the method of THR still has certain reference significance.

B. Ability of Cross-Subject

A cross-subject experiment was additionally performed to further investigate the performance between these recognition systems. Except for the training data set, the experimental process was the same as in the previous experiment. Group B participants' data were excluded from the training data set, which used only group A members' data (this part of the data was the same as the original data). In addition, recognition effect of THR for known data is qualified, but the recognition effect for cross-subjects is very poor, which leads to its low universality. Due to these shortcomings of THR, we only do cross-subject experiments on the recognition system based on the other three algorithms and they are all off-line. Of course, the test data used in the cross-subject experiment is the same as the test data above, which is still the data of the IMUs signals of the three members of group B (S1, S2, and S3) traveling laterally in "Normal speed" mode.

The experimental results are shown in Table IV. The total recognition accuracy (mean and SEM, cross-subjects) of RF-based, UBI-based, and NN-based systems is 91.72% ± 0.42%, 89.63% ± 0.48%, and 89.60% ± 0.43%, respectively. For RF-based system, the recognition accuracy of WDS in lateral gait phase is the worst (88.91% ± 1.12%), the most conspicuous errors were: NDS was misidentified as SLL (7.61% ± 1.43%), SLL was mistaken for WDS (4.53% ± 0.45%), WDS was

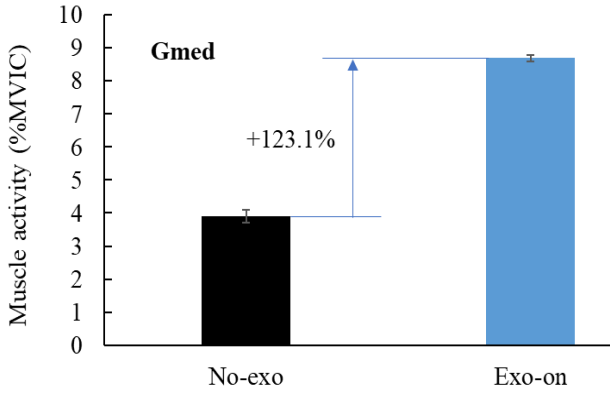

Fig. 12. GMed muscle activities under different lateral walking conditions.

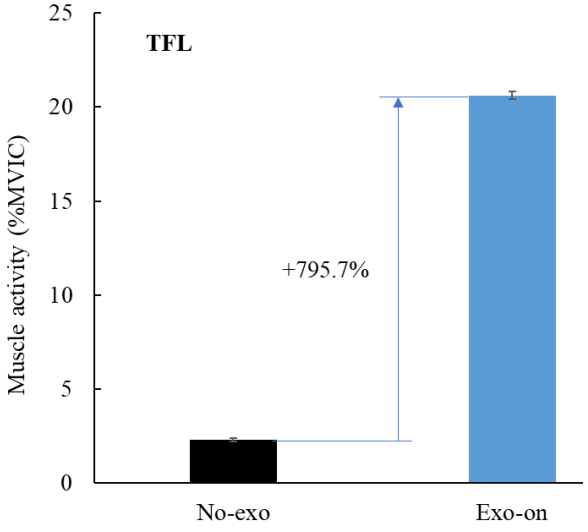

Fig. 13. TFL muscle activities under different lateral walking conditions.

mistaken for SLL (4.97% ± 0.38%), and STL (6.12% ± 1.02%), STL was mistaken for WDS (5.16% ± 1.67%); For UBI-based systems, the recognition accuracy of SLL is the worst (88.36% ± 1.06%), the most conspicuous errors were: NDS was mistaken for SLL (10.35% ± 2.93%), SLL was mistaken for WDS (7.81% ± 1.76%), and STL was mistaken for WDS (6.16% ± 0.84%); For the NN-based system, the recognition accuracy of NDS is the worst (84.93% ± 2.14%), the most conspicuous errors were: NDS was mistaken for SLL (9.24% ± 1.42%), WDS was mistaken for SLL (5.84% ± 1.13%), and STL (6.33% ± 1.40%).

Visualizing the feature vectors in 2-D spaces, as shown in Fig. 11, with the blue, green, orange, and fuchsia sections representing the feature vectors of the NDS, SLL, WDS, and STL, respectively, and the "◯" representing the correct classification points, "×", "+," and "∗" represent classification points of error ("×" and "+" denote mistaken for adjacent classes, "∗" denote mistaken for alternating classes). The ERR1 and ERR2 were unavoidable since the borderline may not be clear. However, for ERR3, the algorithm can be improved according to the characteristics of the lateral gait is quasi-periodic, so as to reduce the occurrence of ERR3.

Although the dimensionality reduction of multidimension feature vector results in the loss of information, the 2-D graph can intuitively show the relative positions of different phases in space. It is easy to find that in the 2-D graph of S1, S2, and S3, the distribution of feature vector corresponding to different phases of gait is approximately the same, as shown in Fig. 11.

We used the results of no cross-subject experiment as a control group. And put it together with the results of cross-subject experiments to draw a histogram. This can intuitively compare the differences between the no cross-subject experiment and the cross-subject experiment. As shown in Fig. 10, compared to no cross-subject experiments, the recognition accuracy of the UBI system decreased the most (7.01%) in cross-subject experiment. The recognition accuracy of RF and NN systems decreased by about the same amount (about 5.5%). This trend is consistent with the findings of Zhang et al. [30] and Rosa et al. [31].

C. Muscle Activity

We also conducted an experiment to assess the effect of the hip exoskeletons on wearers in muscle activity. The muscle activity of GMed and TFL of five subjects were recorded. The trials include lateral walking No-exo and lateral walking Exo-on. The resistance force is set to be 7 nm. Each subject has a 30-min rest after each trial. The muscle activity was presented as a percentage of the MVIC (% MVIC) [32]. EMG data collected during the target resistance torque phase were normalized to their muscles' respective MVIC trials and therefore expressed as % MVIC. The result of muscle activity is reported in the form of the mean ± SEM. The effects of different conditions on the muscle activity were analyzed using ANOVA. Differences among walking conditions were assessed using the two-sided paired t-tests.

The GMed muscle activities in No-exo and Exo-on conditions were 3.9% ± 0.2%MVIC and 8.7% ± 0.1%MVIC (mean ± SEM), respectively. The corresponding increment in the Exo-on condition was 123.1% (refer to Fig. 12).

The TFL muscle activities in No-exo and Exo-on conditions were 2.3% ± 0.1%MVIC and 20.6% ± 0.2%MVIC (mean ± SEM), respectively. The corresponding increment in the Exo-on condition was (refer to Fig. 13).

D. Limitation

Although the proposed gait phase recognition method can be used in lateral walking, a number of limitations of this work exist. First, the effect of the number of subjects or the number of feature vector on the accuracy of the identification system was not explored. The methods of Gu et al. [33] may be used in the future work. Second, the recognition results under different locomotion modes also deserve to be studied. Finally, since the need to use the same test data to compare the performance of different recognition systems, only one system is real-time. Finally, more advanced control strategies [34], [35] will be researched for the exoskeleton.

V. Conclusion

In this work, we presented a method for lateral walking gait phase detection only by two IMUs mounted on the shank.

A hip exoskeleton applied to lateral resistance walking was developed. Experiments were conducted to detect four lateral walking gait phases at various speeds. The performance of four different algorithms was evaluated. The results demonstrated that the time, space, and accuracy performance of the method met the requirements of lateral walking. It can be used to develop wearable exercise devices for lateral walking gait. This article is a report of the initial exploration of the application of the lateral exoskeleton. Later in the project, IMUs will be designed to be mounted on the lateral exoskeleton.

REFERENCES

[1] C. L. Lewis, H. D. Foley, T. S. Lee, and J. W. Berry, "Hip-muscle activity in men and women during resisted side stepping with different band positions," *J. Athletic Training*, vol. 53, no. 11, pp. 1071–1081, Nov. 2018.

[2] Y. Sun, Y. Tang, J. Zheng, D. Dong, X. Chen, and L. Bai, "From sensing to control of lower limb exoskeleton: A systematic review," *Annu. Rev. Control*, vol. 53, pp. 83–96, 2022.

[3] J. Kim et al., "Reducing the metabolic rate of walking and running with a versatile, portable exosuit," *Science*, vol. 365, no. 6454, pp. 668–672, Aug. 2019.

[4] X. Chen, K. Zhang, H. Liu, Y. Leng, and C. Fu, "A probability distribution model-based approach for foot placement prediction in the early Swing phase with a wearable IMU sensor," *IEEE Trans. Neural Syst. Rehabil. Eng.*, vol. 29, pp. 2595–2604, 2021.

[5] X. Zhang et al., "Gait pattern identification and phase estimation in continuous multilocomotion mode based on inertial measurement units," *IEEE Sensors J.*, vol. 22, no. 17, pp. 16952–16962, Sep. 2022.

[6] B. Zhong, K. Guo, H. Yu, and M. Zhang, "Toward gait symmetry enhancement via a cable-driven exoskeleton powered by series elastic actuators," *IEEE Robot. Autom. Lett.*, vol. 7, no. 2, pp. 786–793, Apr. 2022.

[7] A. Sant'Anna and N. Wickström, "A symbol-based approach to gait analysis from acceleration signals: Identification and detection of gait events and a new measure of gait symmetry," *IEEE Trans. Inf. Technol. Biomed.*, vol. 14, no. 5, pp. 1180–1187, Sep. 2010.

[8] E. D. Ledoux, "Inertial sensing for gait event detection and transfemoral prosthesis control strategy," *IEEE Trans. Biomed. Eng.*, vol. 65, no. 12, pp. 2704–2712, Dec. 2018.

[9] J. Bruinsma and R. Carloni, "IMU-based deep neural networks: Prediction of locomotor and transition intentions of an osseointegrated transfemoral amputee," *IEEE Trans. Neural Syst. Rehabil. Eng.*, vol. 29, pp. 1079–1088, 2021.

[10] A. R. Anwary, H. Yu, and M. Vassallo, "Optimal foot location for placing wearable IMU sensors and automatic feature extraction for gait analysis," *IEEE Sensors J.*, vol. 18, no. 6, pp. 2555–2567, Mar. 2018.

[11] G. Panahandeh, N. Mohammadiha, A. Leijon, and P. Händel, "Continuous hidden Markov model for pedestrian activity classification and gait analysis," *IEEE Trans. Instrum. Meas.*, vol. 62, no. 5, pp. 1073–1083, May 2013.

[12] T. Fang, W. Cao, C. Chen, Y. Zhang, Z. Wang, and X. Wu, "A soft exosuit for hip extension assistance of the elderly," *Technol. Health Care*, vol. 29, no. 4, pp. 837–841, Jul. 2021.

[13] D. Shin, S. Lee, and S. Hwang, "Locomotion mode recognition algorithm based on Gaussian mixture model using IMU sensors," *Sensors*, vol. 21, no. 8, p. 2785, Apr. 2021.

[14] Y. Sun, X. Xu, X. Tian, L. Zhou, and Y. Li, "An adaptive zero-velocity interval detector using instep-mounted inertial measurement unit," *IEEE Trans. Instrum. Meas.*, vol. 70, 2021, Art. no. 8502013, doi: 10.1109/TIM.2021.3065508.

[15] D. Yamashita, K. Fujii, S. Yoshioka, T. Isaka, and M. Kouzaki, "Asymmetric interlimb role-sharing in mechanical power during human sideways locomotion," *J. Biomechanics*, vol. 57, pp. 79–86, May 2017.

[16] J. W. Berry, T. S. Lee, H. D. Foley, and C. L. Lewis, "Resisted side stepping: The effect of posture on hip abductor muscle activation," *J. Orthopaedic Sports Phys. Therapy*, vol. 45, no. 9, pp. 675–682, Sep. 2015.

[17] G. Kuntze, W. I. Sellers, and N. Mansfield, "Bilateral ground reaction forces and joint moments for lateral sidestepping and crossover stepping tasks," *J. Sport. Sci. Med.*, vol. 8, no. 1, pp. 1–8. Mar. 2009.

[18] E. Zheng, S. Manca, T. Yan, A. Parri, N. Vitiello, and Q. Wang, "Gait phase estimation based on noncontact capacitive sensing and adaptive oscillators," *IEEE Trans. Biomed. Eng.*, vol. 64, no. 10, pp. 2419–2430, Oct. 2017.

[19] L. Breiman, "Random forests," *Mach. Learn.*, vol. 45, no. 1, pp. 5–32, 2001.

[20] L. E. Raileanu and K. Stoffel, "Theoretical comparison between the Gini index and information gain criteria," *Ann. Math. Artif. Intell.*, vol. 41, no. 1, pp. 77–93, May 2004.

[21] A. K. Godiyal, M. Mondal, S. D. Joshi, and D. Joshi, "Force myography based novel strategy for locomotion classification," *IEEE Trans. Hum.-Mach. Syst.*, vol. 48, no. 6, pp. 648–657, Dec. 2018.

[22] D. Xu and Q. Wang, "On-board training strategy for IMU-based real-time locomotion recognition of transtibial amputees with robotic prostheses," *Frontiers Neurorobotics*, vol. 14, p. 47, Oct. 2020, doi: 10.3389/fnbot.2020.00047.

[23] C. Hershler and M. Milner, "An optimality criterion for processing electromyographic (EMG) signals relating to human locomotion," *IEEE Trans. Biomed. Eng.*, vols. BME–25, no. 5, pp. 413–420, Sep. 1978.

[24] J. Ryu, B.-H. Lee, J. Maeng, and D.-H. Kim, "SEMG-signal and IMU sensor-based gait sub-phase detection and prediction using a user-adaptive classifier," *Med. Eng. Phys.*, vol. 69, pp. 50–57, Jul. 2019.

[25] L.-F. Shi, C.-X. Qiu, D.-J. Xin, and G.-X. Liu, "Gait recognition via random forests based on wearable inertial measurement unit," *J. Ambient Intell. Humanized Comput.*, vol. 11, no. 11, pp. 5329–5340, Nov. 2020.

[26] H. Huang, P. Zhou, Y. Li, and F. Sun, "A lightweight attention-based CNN model for efficient gait recognition with wearable IMU sensors," *Sensors*, vol. 21, no. 8, pp. 1–13, Apr. 2021.

[27] M. A. M. Hasan, F. A. Abir, M. A. Siam, and J. Shin, "Gait recognition with wearable sensors using modified residual block-based lightweight CNN," *IEEE Access*, vol. 10, pp. 42577–42588, 2022.

[28] N. C. Bejarano, E. Ambrosini, A. Pedrocchi, G. Ferrigno, M. Monticone, and S. Ferrante, "A novel adaptive, real-time algorithm to detect gait events from wearable sensors," *IEEE Trans. Neural Syst. Rehabil. Eng.*, vol. 23, no. 3, pp. 413–422, May 2015.

[29] J. Rueterbories, E. G. Spaich, and O. K. Andersen, "Gait event detection for use in FES rehabilitation by radial and tangential foot accelerations," *Med. Eng. Phys.*, vol. 36, no. 4, pp. 502–508, 2014.

[30] K. Zhang, J. Wang, C. W. de Silva, and C. Fu, "Unsupervised cross-subject adaptation for predicting human locomotion intent," *IEEE Trans. Neural Syst. Rehabil. Eng.*, vol. 28, no. 3, pp. 646–657, Mar. 2020.

[31] L. G. Rosa, J. S. Zia, O. T. Inan, and G. S. Sawicki, "Machine learning to extract muscle fascicle length changes from dynamic ultrasound images in real-time," *PLoS One*, vol. 16, no. 5, pp. 1–17, May 2021.

[32] J. W. Youdas et al., "Electromyographic analysis of trunk and hip muscles during resisted lateral band walking," *Physiotherapy Theory Pract.*, vol. 29, no. 2, pp. 113–123, Feb. 2013.

[33] X. Gu, Y. Guo, F. Deligianni, B. Lo, and G.-Z. Yang, "Cross-subject and cross-modal transfer for generalized abnormal gait pattern recognition," *IEEE Trans. Neural Netw. Learn. Syst.*, vol. 32, no. 2, pp. 546–560, Feb. 2021.

[34] C. Huang, Z. Lai, X. Wu, and T. Xu, "Multimodal locomotion and cargo transportation of magnetically actuated quadruped soft microrobots," *Cyborg Bionic Syst.*, vol. 2022, no. 4, pp. 1–10, Dec. 2022.

[35] T. Xu, C. Huang, Z. Lai, and X. Wu, "Independent control strategy of multiple magnetic flexible millirobots for position control and path following," *IEEE Trans. Robot.*, vol. 38, no. 5, pp. 2875–2887, Oct. 2022.

Lijun Yang received the B.S. degree in automation from Guangxi University, Nanning, China, in 2020. He is currently pursuing the M.S. degree in automation with the Wuhan University of Technology, Wuhan, China.

He is also a Visiting Student with the Shenzhen Institute of Advanced Technology, Chinese Academy of Sciences, Shenzhen, China. His research interests are lower limb exoskeletons and control strategy.

Kui Xiang received the Ph.D. degree from the School of Electrical Engineering, Zhejiang University, Hangzhou, China, in 2006.

He was promoted to Professor at the Wuhan University of Technology, Wuhan, China, in 2014. His research interests include optimal design and intelligent control of wearable robots and legged robots.

Dr. Xiang currently serves as a member of the Intelligent Robot Professional Committee of the Chinese Artificial Intelligence Society.

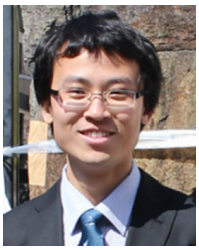

Muye Pang received the Ph.D. degree from the National Xiangchuan University of Japan, in 2015.

He was promoted to Associate Professor at the Wuhan University of Technology, Wuhan, China, in 2017. His research interests include optimization design and intelligent control of robot systems for social services.

Dr. Pang serves as a member of the Intelligent Robot Professional Committee of the Chinese Artificial Intelligence Society.

Meng Yin received the Ph.D. degree from the State Key Laboratory of Robotics, Chinese Academy of Sciences, University of Chinese Academy of Sciences in China, Beijing, China.

He is currently a Senior Engineer with the Shenzhen Institutes of Advanced Technology, Chinese Academy of Sciences, Shenzhen, China. His research interest includes tendon-sheath driven humanoid robots.

Xinyu Wu (Senior Member, IEEE) received the B.E. and M.E. degrees from the Department of Automation, University of Science and Technology of China, Hefei, China, in 2001 and 2004, respectively, and the Ph.D. degree from the Chinese University of Hong Kong, Hong Kong, in 2008.

He is currently a Professor at the Shenzhen Institute of Advanced Technology, Chinese Academy of Sciences, Shenzhen, China. He is the director of Center for Intelligent Bionic. He has published over 180 articles and two monographs. His research interests include computer vision, robotics, and intelligent system.

Wujing Cao received the Ph.D. degree from Rehabilitation Engineering and Technology Institute, University of Shanghai for Science and Technology, Shanghai, China, in 2019.

He is currently an Associate Research Fellow at the Shenzhen Institute of Advanced Technology, Chinese Academy of Sciences, Shenzhen, China. His research interests include lower limb exoskeleton and microprocessor-controlled prosthetic knee.